INTERNATIONAL JOURNAL OF HYDROGEN ENERGY 45 (2020) 25249–25261

Available online at www.sciencedirect.com

ScienceDirect

journal homepage: www.elsevier.com/locate/he

Comparative study on the resistance of different catalysts to electrochemical damage of fuel cells

Yi-Nan Nie, Lei Chen*, Wen-Quan Tao

Key Laboratory of Thermo-Fluid Science and Engineering of MOE, School of Energy and Power Engineering, Xi'an Jiaotong University, Xi'an, Shaanxi, 710049, China

HIGHLIGHTS

- Propose the concept that SO3- interferes with the electrochemical reaction in FC.
- Model the electrochemical reaction under the interference of SO3- by DFT method.
- Propose catalyst selection principle considering anti-interference performance.

ARTICLE INFO

Article history:
Received 9 March 2020
Received in revised form
6 June 2020
Accepted 11 June 2020
Available online 6 August 2020

Keywords:
Fuel cell
Electrochemical damage
Catalytic performance
DFT calculation

ABSTRACT

This paper studies the catalytic performance and resistance to electrochemical damage of different catalysts in fuel cells by DFT calculations. The most commonly used platinum particle catalysts (Pt (111) surface) and three kinds of graphene-based platinum single-atom catalysts (G-N1-Pt, G-N2-Pt and G-N4-Pt) are selected as research objects. Based on Norskov's classical electrochemical theory, the step diagrams of hydrogen oxidation reaction (HOR) and oxygen reduction reaction (ORR) under the standard reaction conditions and the interference with the addition of SO_3^- groups are calculated. Combined with the actual adsorption situation in the intermediate steps of the reaction, the catalytic performance of the standard reaction and the catalytic performance under the interference of SO_3^- groups are compared. For HOR reaction and ORR reaction, the catalysts with the best catalytic ability and anti-interference ability are G-N1-Pt catalyst and G-N2-Pt catalyst, respectively. A catalyst selection principle that balances activation performance and anti-interference performance in fuel cells is proposed.

Introduction

Today, hydrogen is considered one of the most promising alternatives to fossil energy. In the use of hydrogen energy, fuel cells have attracted extensive interest due to their environmental friendliness, high energy density, and low noise [1]. A fuel cell is a device that converts the chemical energy of an active substance into electrical energy [2].

For a fuel cell, the membrane electrode assembly is the most important working component [3]. It is formed by hot-pressing two gas diffusion layers (GDL), two catalytic layers (CL) and a proton exchange membrane (PEM), and is held and fixed by a bipolar plate on both sides during operation. A fuel cell is an energy converter with a simple working principle. In theory, as long as the active materials such as fuel and oxidant are continuously input and the products can be eliminated in

* *Corresponding author.*
E-mail address: chenlei@mail.xjtu.edu.cn (L. Chen).
https://doi.org/10.1016/j.ijhydene.2020.06.100

time, the fuel cell can continuously generate electricity. However, it is well known that any equipment has its working life, and the working life of fuel cells is generally thousands of hours [4]. There are many reasons for fuel cell failure, such as thermal damage, mechanical damage, and electrochemical damage [5–9]. Further expanding these causes are thermal stress, mechanical stress, catalyst migration, catalyst poisoning, and so on.

As mentioned, the fuel cell is a kind of energy converter based on hydrogen oxidation reaction (HOR) [10,11] and oxygen reduction reaction (ORR) [12,13]. The basic reactions in a fuel cell are as follows [14]:

$$\text{Anode: } H_2 \rightarrow 2H^+ + 2e^- \quad (1)$$

$$\text{Cathode: } 2H^+ + 2e^- + \frac{1}{2}O_2 \rightarrow H_2O \quad (2)$$

$$\text{Overall: } H_2 + \frac{1}{2}O_2 \rightarrow H_2O \quad (3)$$

In a proton exchange membrane fuel cell, hydrogen is decomposed into protons and electrons at the anode catalytic layer, the protons move to the cathode through the proton exchange membrane, and the electrons enter the cathode after passing through an external circuit. Protons, electrons and oxygen react together at the cathode catalytic layer to produce water. It can be seen that in the normal working process, the regions where the hydrogen oxidation reaction (HOR), the oxygen reduction reaction (ORR), and the proton transfer occur in the membrane electrode assembly are very certain, and the division of labor between the components is clear.

However, after a period of work, the internal structure of the fuel cell membrane electrode assembly will be damaged to some extent. In order to discuss this phenomenon, we conduct relevant experiments. The experimental steps are as follows:

(1) The temperature of the fuel cell and the temperature of the dew point humidifier are stabilized for 1–2 h. Before the temperature is stabilized, the reaction gas is discharged through the bypass without passing into the fuel cell. When the temperature is stable, the bypass is closed alternately, and the reaction gas is passed into the fuel cell.
(2) The membrane electrode assembly is operated at a current density of 0.4 $A \cdot m^{-2}$ for 1 h to completely wet it, and the influence of the previous operation on the internal state of the membrane electrode assembly is eliminated by this step.
(3) After the above two steps, the working conditions of the fuel cell and the initial state of the membrane electrode assembly have been stabilized, and the conditions for continuous operation for a long time have been met. The current density is circulated in the range of 0–1 $A \cdot cm^{-2}$ with a current step size of 0.1 $A \cdot cm^{-2}$ to maintain the continuous operation of the fuel cell. In this article, the total operating time of the fuel cell is 20 h.

After 20 h operation, the arrangement of the components in the membrane electrode assembly, which is originally regular and complete (as shown in Fig. 1(a)), tends to be chaotic (as shown in Fig. 1(b)). As can be seen from Fig. 1(a), the unworking membrane electrode assembly shows the basic structure of GDL-(CL)PEM(CL)-GDL (due to the small size of the catalytic layer, it appears to be integrated with the proton exchange membrane in the figure), the outer boundary of each component is complete and clear. As can be seen from Fig. 1(b), the membrane electrode assembly cross section after 20 h of operation is very chaotic, it is impossible to clearly distinguish the delamination of each component, and the overall structure becomes loose. At this time, the following situations may occur:

(1) The catalytic layer is pierced by carbon fibers in the gas diffusion layer. Since the thickness of the catalytic layer is usually only a few microns, in the case shown in Fig. 1(b), it is easily punctured by GDL carbon fibers in a chaotic state.
(2) With the internal destruction of the membrane electrode assembly and driven by the progress of the internal flow and mass transfer process, the catalyst (platinum particles) in the catalytic layer will move into the proton exchange membrane and agglomerate [15].
(3) The catalytic layer is in direct contact with the proton exchange membrane in the membrane electrode. After prolonged operation, the proton exchange membrane and the catalytic layer will be destroyed, and the interface between the two layers of components cannot be maintained. At this time, the composition between the two components will be blended with each other.

In the above three cases, it will cause a certain change in the electrochemical reaction environment inside the membrane electrode assembly. In case (1), the punctured part of the catalytic layer will be completely destroyed, and the destroyed part cannot carry out the electrochemical reaction, and it will also prevent the diffusion of the working gas. In case (2), the electrochemical reaction will be affected because the loss of catalyst will lead to a decrease in the area of catalytic activity, which further leads to a decline in fuel cell performance. In case (3), the catalytic layer is blended with the proton exchange membrane components, or within a certain scale on the surface of the proton exchange membrane, the interface between the catalytic layer and the proton exchange membrane is blurred. In this case, the damage to the catalytic layer is much higher than the damage to the proton exchange membrane. The structure of the proton exchange membrane on the microstructure will be mixed with the structure of the catalytic layer to destroy the environment of the electrochemical reaction. Proton exchange membrane materials mostly use Nafion invented by Dupont Corporation. This material is a typical polymer material whose molecular chain

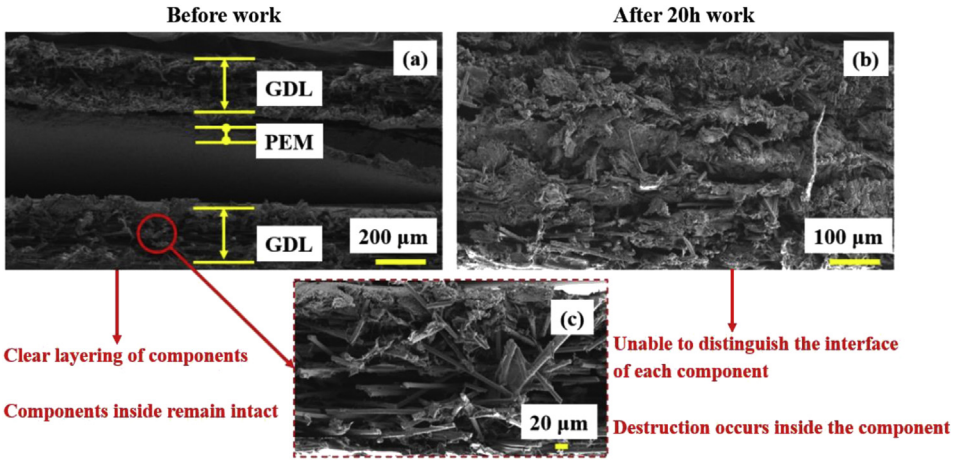

Fig. 1 – Comparison of the cross-section of the non-working membrane electrode assembly (a) and the membrane electrode assembly after 20 h of operation (b).

is composed of fluorocarbon main chain and sulfonate branched chain [16]. Under the above circumstances, the SO_3^- group at the top of the sulfonate branch in Nafion will have the greatest impact on the environment of the electrochemical reaction site. It is weakly bonded to the main bond in the molecular chain and it is located on the periphery of the molecular chain as a branch chain, which is liable to contact with the internal structure of the catalytic layer. And it also mentioned in the lierature that SO_3^- group may degrade from Nafion under high temperature conditions [17]. The most crucial part is that the oxygen atom at the top of the SO_3^- group easily reacts and adsorbs with the platinum atom at the active site in the catalyst. In such cases, it is very likly to have a great influence on the intermediate steps of the electrochemical reaction.

Therefore, the electrochemical damage in this article refers specifically to the interference of the SO_3^- group. This article aims to establish a background of actual adsorption situation, which is different from the general catalyst performance research. We hope to study the performance of the catalyst under interference and simulate the conditions that may be encountered during the actual operation of the fuel cell to propose the catalyst anti-interference performance analysis providing suggestions and references for catalyst design and selection.

Aiming at the above problems, this paper studies the electrochemical reaction of different catalysts under the interference of SO_3^- groups and compares their anti-interference ability.

Details of numerical simulation

Calculation methods and models

This paper mainly uses the following software packages for modeling and calculation: Material Studio is mainly used to build physical models [18]. VASP, developed by the Hafner team at the University of Vienna, is mainly used for DFT calculations [19]. The VASPKIT software package, written by a team of Pro. Wang Wei, Dr. Xu Nan and Dr. Liu Jincheng, is used for post-processing of VASP calculation results [20]. VESTA software is used to visualize the structure files [21].

In this paper, the traditional platinum particle catalyst and three graphene-based single-atom catalysts (G-N1-Pt, G-N2-Pt, and G-N4-Pt) are studied. The catalyst surface modeling process is described below.

Currently, platinum-based catalysts are widely used in proton exchange membrane fuel cells. The catalysts studied in this paper include traditional platinum particle catalysts (Pt (111) crystal plane surface is usually selected as the catalytic surface) and recently emerging single-atom catalysts [22–24].

For traditional platinum particle catalyst surface modeling, platinum metal crystal plane is selected as the catalyst surface model. The crystal structure model in the 'pure-metals' library of Materials Studio is used where lattice parameter is 0.3924 nm. After importing the Pt bulk model in Materials Studio, use 'Cleave Surface' option to cut it along the (1 1 1) direction, 4 layers of atoms are intercepted as the representation model of Pt (111) surface [25–27]. Use 'Build Vacuum Slab' option sets the vacuum layer thickness to 15 Å, which ensures the following three points: (1) The thickness of the vacuum layer should allow sufficient free distances between surface atoms without affecting the surface relaxation; (2) It is necessary to sufficiently eliminate the interaction between adjacent surface atoms; (3) When studying the adsorption of molecules, there is enough space for the molecules to move freely.

The three single-atom catalysts studied in this paper are all based on graphene, while nitrogen doping on the basis of graphene as platinum atom substrate. Three single-atom catalysts are selected in this paper, with one, two, and four doping nitrogen atoms as the substrate, and named G-N1-Pt, G-N2-Pt, and G-N4-Pt (G represents graphene).

The three catalyst structures of G-N1-Pt, G-N2-Pt and G-N4-Pt are nitrogen-doped graphene single-atom catalyst structures that are relatively simple in the actual construction process in literature reports, relatively liable to prepare and realize, and have better application prospects, so this article

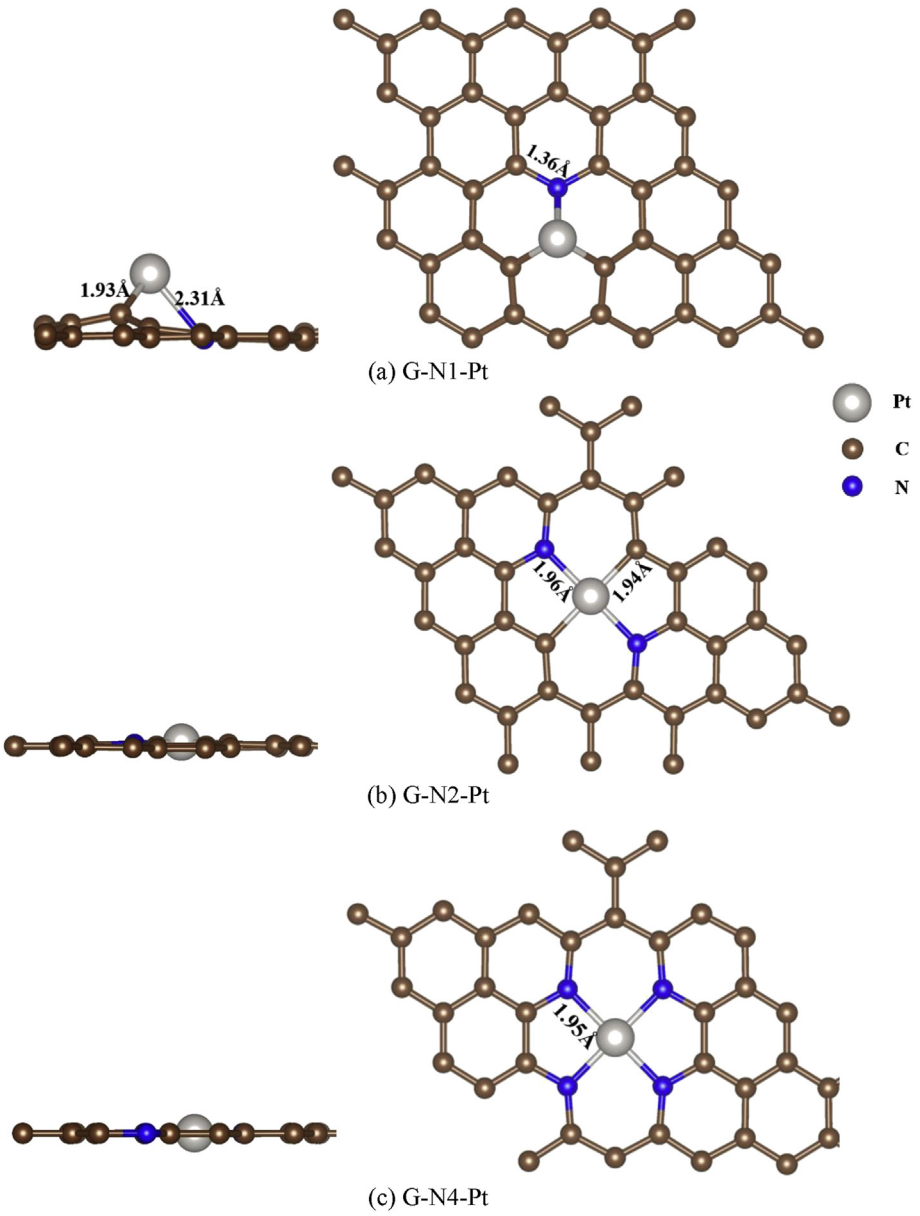

Fig. 2 – Top view of G-N1-Pt (a), G-N2-Pt (b) and G-N4-Pt (c) catalyst structures.

selects these three structures for research. Among them, the structure of G-N1-Pt catalyst is proposed by Fei H [28]. G-N2-Pt and G-N4-Pt catalysts are proposed based on the existing similar single-atom catalyst structures of graphene substrates [29]. After the structure optimization, they are both planar structures.

The top view and side view of the three single-atom catalysts are shown in Fig. 2. To build single-atom catalysts models, the graphene structures of the Materials Studio structure library are expanded into 2 × 2 supercells, some carbon atoms are deleted or replaced with doped nitrogen atoms as needed to artificially create internal defects in graphene, then platinum atom is placed in the defects as the initial structure of the catalyst model. For the G-N2-Pt and G-N4-Pt catalysts, we place the platinum atoms at different heights as the initial configuration during the calculation. After the calculation, the planar configurations are obtained, and the configuration reliability is guaranteed. A vacuum layer with a thickness of 15 Å is built.

The PAW-GGA-PBE potential that comes with the VASP software package is selected for the platinum, hydrogen, and oxygen elements. Before calculating the electrocatalysis and adsorption on the surface of each catalyst, the structure of the surface model of each catalyst is optimized to obtain its system energy. The main calculation parameter settings of VASP can be seen in Table 1.

By placing hydrogen atoms in the initial position of platinum atoms above 1.4 Å, the adsorption model of hydrogen atoms on the top of platinum is completed. For ORR reactions, the adsorption sites of all intermediate adsorbents are directly set up on the platinum atom site using Materials Studio.

For different catalysts, when considering the effect of SO_3^- groups on the reaction, there will be some differences in the

Table 1 – The main calculation parameter settings of VASP.

	Calculation of adsorption system	Thermodynamic correction calculation
Plane wave truncation energy/eV	ENCUT = 500	ENCUT = 500
Fractional orbit processing algorithm	ISMEAR = 0, SIGMA = 0.05	ISMEAR = 0, SIGMA = 0.05
Convergence algorithm	Conjugate gradient algorithm	Finite difference method
	IBRION = 2, POTIM = 0.2	IBRION = 5, POTIM = 0.015
Scf iteration accuracy/eV	EDIFF = 1×10^{-6}	EDIFF = 1×10^{-7}

model building method. In the calculation, it can be found that the position and angle of the SO_3^- group placement have little effect on the state of the final reaction system. The key is the distance between the SO_3^- group and the active site of the catalyst. The basic idea is to place an SO_3^- group within 1–2 Å distance (ensure that the top oxygen atom and the active site may form a bond) range near the adsorption site to build an initial model. Because the SO_3^- group has a triangular pyramid structure with sulfur atoms as the apex, and the sulfur atom is connected to the branch chain in Nafion, the oxygen atom should be placed as close to the adsorption site as possible when building the model.

Computation of electrochemical reactions

As mentioned in the introduction, the work of a proton exchange membrane fuel cell is based on its internal electrochemical reaction, and the electrochemical reaction mainly occurs in the anode and cathode inside the membrane electrode assembly. Hydrogen oxidation reaction (HOR) and oxygen reduction reaction (ORR) occur in the two electrodes of the membrane electrode assembly.

In the fuel cell anode reaction and the cathode reaction, the HOR reaction process of the anode is relatively simple. The process is that hydrogen (H_2) is decomposed into two hydrogen atoms and adsorbed on the catalyst surface (H*). Then the hydrogen atom desorbs into hydrogen ions (H^+) and electrons (e^-) to complete the reaction. The reaction process is as follows:

$$\begin{aligned} &1e{:}^* + H_2 \rightarrow 2H^* \\ &2e: 2H^* \rightarrow {}^* + 2H^+ + 2e^- \end{aligned} \tag{4}$$

where: * represents catalyst surface, and H^* represents that the catalyst surface with one hydrogen atom adsorbed.

Based on Norskov's classical electrocatalytic calculation method [25–27], for the electrocatalytic calculation, it is not necessary to calculate the transition state, and only the energy of the intermediate must be calculated while taking into account the contribution of electric charge. Then modeling the electrochemical reaction of proton exchange membrane fuel is to model the reaction of HOR reaction and ORR reaction step by step. Because the HOR reaction process is simple and its reaction is mainly based on the adsorption of hydrogen atoms by the catalyst, the most important part of modeling the fuel cell electrochemical reaction is to calculate the electrochemical adsorption process of each step of the cathode ORR reaction.

For proton exchange membrane fuel cells, the choice of catalyst type plays a key role in its electrochemical performance. For the HOR reaction, the adsorption capacity of the hydrogen atom on the catalyst surface determines its reaction capacity. According to the theory of Norskov, the hydrogen atom adsorption energy formula in the HOR reaction is [26]:

$$\Delta E_H = \frac{1}{n}\left(E(\text{surf}+n\text{H}) - E(\text{surf}) - \frac{n}{2}E(\text{H}_2)\right) \tag{5}$$

where: ΔE_H represents the hydrogen atom adsorption energy, n represents the number of hydrogen atoms in the adsorption system, surf represents the adsorption surface system.

Based on the hydrogen atom adsorption energy, the free energy of the adsorption system can be further calculated:

$$\Delta G_{H^*} = \Delta E_H + \Delta E_{ZPE} - T\Delta S_H \tag{6}$$

where: ΔG_{H^*} is the free energy of the adsorption system, ΔE_{ZPE} is the zero energy difference between the adsorption state and the gas phase state, according to the literature, 0.04eV, T is the temperature of reaction system, ΔS_H is the vibration entropy of the hydrogen atom, $\Delta S_H \cong -1/2S^0_{H_2}$, and $S^0_{H_2}$ is the entropy value of the hydrogen molecule in the standard gas. Based on the above, the above formula can be simplified into [27]: $\Delta G_{H^*} = \Delta E_H + 0.24\text{eV}$.

There are several intermediate processes in the ORR reaction of the cathode, the initial state of the standard ORR reaction includes one oxygen molecule (O_2) and two hydrogen molecules (H_2). The oxygen molecules are adsorbed on the catalyst surface and combine with the hydrogen atoms in a hydrogen molecule to form a hydrogen peroxide (OOH^-). The hydroxide (OH^-) in the hydrogen peroxide (OOH^-) is combined with a hydrogen atom to form a water molecule. At this time, an oxygen atom is adsorbed on the catalyst surface. Then the adsorbed oxygen atom combines with the hydrogen atom in another hydrogen molecule to form hydroxide (OH^-) adsorbed on the catalyst surface. Finally, the hydroxide is desorbed from the surface of the catalyst, and combines with independent hydrogen atoms to form another water molecule (H_2O).

$$\begin{aligned} &1e{:}^* + H_2 + \frac{1}{2}O_2 \rightarrow {}^*OOH^- + H^+ \\ &2e{:}^*OOH^- + H^+ \rightarrow {}^*O + H_2O \\ &3e{:}^*O + H_2O \rightarrow {}^*OH^- + OH^- \\ &4e{:}^*OH^- + OH^- \rightarrow {}^* + H_2O + O \end{aligned} \tag{7}$$

For an ideal ORR reaction, the energy step (overpotential) corresponding to each electrochemical reaction step should be 1.23 eV. In the actual process, the overpotential of each electrochemical reaction step is different, and the overall reaction overpotential is always maintained at 4.92 eV. Since the

overpotential of each intermediate reaction does not perfectly match 1.23 eV, the difference between the actual overpotential and the ideal overpotential is called the overpotential drop (η). The performance of electrocatalytic materials is largely determined by the maximum overpotential drop in their participation in chemical reactions. A good electrocatalyst should reduce the overpotential of the electrochemical reaction step with the highest overpotential as much as possible, which can reduce the overall electrochemical reaction barriers. According to the calculation method of overpotential proposed by Norskov, the overpotential drop formula is [27]:

$$\eta = U - U^{eq} \tag{8}$$

Where: η is the overpotential drop, U is the actual electrode potential, and U^{eq} is the theoretical equilibrium potential. According to the above-mentioned four-step intermediate reaction process, the corresponding overpotential calculation method of each step is as follows:

$$\begin{aligned}
\Delta G(1) &= G(^{*}OOH^{-}) + G(3/2H_2) - G(^{*}) - G(2H_2) - G(O_2)\\
\Delta G(2) &= G(^{*}O) + G(H_2O) + G(H_2) - G(^{*}OOH^{-}) - G(3/2H_2)\\
\Delta G(3) &= G(^{*}OH^{-}) + G(H_2O) + G(H^{+}) - G(^{*}O) - G(H_2O) - G(H_2)\\
\Delta G(4) &= G(^{*}) + G(H_2O) - G(^{*}OH^{-}) - G(H_2O) - G(H^{+})
\end{aligned} \tag{9}$$

where: * represents the catalyst surface model (activation site).

Analysis of calculation results

HOR reaction analysis

For electrochemical reactions, a common method of analysis is to use a step diagram to analyze. The basis of this analysis method is based on Norskov's classical electrocatalytic calculation method for electrocatalytic calculation: there is no need to calculate the transition state, only the energy of the intermediate needs to be considered with the contribution of electric charge [27]. The basic idea of the step diagram is to take the system in the initial state of the reaction as the zero point, and treat the system free energy of each intermediate reaction step in the reaction as a step, and connect the free energy steps of the reaction system of each step through the free energy step. The trend of the system can be seen in the energy trend of the reaction process, so the overall situation of the reaction can be analyzed [26,27]. The x-axis of the step diagram has no practical significance, and only represents different intermediate reaction systems. The direction to the right is the reaction process. The middle reaction system corresponding to each step is marked in the figure. The points in the figure are used to distinguish different step polylines.

Table 2 – Hydrogen atom adsorption energy of different catalysts.

	Pt (111)	G-N1-Pt	G-N2-Pt	G-N4-Pt
ΔE_H/eV	−1.462	−1.167	0.37	1.441
ΔE_H with SO_3^-/eV	−1.222	−0.802	0.029	0.162

For HOR reactions, which have only one intermediate reaction step, the analysis process is relatively simple. The calculated values of the apex adsorption energy of different catalysts for hydrogen atoms are shown in Table 2. Step diagram of HOR reaction and the change in the free energy of the adsorption system after the addition of SO_3^- is shown in Fig. 3 (as mentioned in 2.2, $\Delta G_{H^*} = \Delta E_H + 0.24eV$).

Generally, a negative or near zero adsorption energy indicates that the adsorption system is more stable. It can be seen from Fig. 3(a) that when calculating the adsorption energy, the performances of the two catalysts, Pt (111) and G-N1-Pt perform best, G-N2-Pt performs next, and G-N4-Pt presents the worst. When interfering SO_3^- groups are placed in the system, the performance of catalysts under the action of each catalyst changes greatly (as shown in Fig. 3(b)).

For the HOR reaction, the free energy of the intermediate reaction should be as close as possible or less than 0 eV, which means that the energy barrier to be overcome during the process is as small as possible. From the above analysis, we can know that in the normal reaction without interference, Pt (111) and G-N1-Pt have the best catalytic effect. The change in the free energy of the reaction after the addition of the SO_3^- group is shown in Fig. 3(b). As can be seen in the figure, the free energy of the Pt (111) catalyst, which originally performed well, has increased significantly, indicating the electrochemical performance decreases under the interference of SO_3^- group. The effect on G-N1-Pt catalyst is less obvious, and the free energy of the reaction has only a slight increase, which does not affect its excellent performance.

In Fig. 3(b), the G-N2-Pt and G-N4-Pt catalysts originally have a high reaction free energy in pure adsorption system, but the free energy decreases significantly under the influence of the SO_3^- group. This has different results from our expectations, which can be explained intuitively when the adsorption systems of four catalysts under the interference of SO_3^- groups are observed (shown in Fig. 4) to further analyze the reaction under interference.

From Fig. 4(a), it is difficult to visually see the effect of SO_3^- group on Pt (111) catalyst, but it can be seen that there are two oxygen atoms in SO_3^- group absorbed to platinum atoms on the surface of Pt (111) catalyst. And the change of the local adsorption system can explain the apparent increase in the free energy of the reaction system after the addition of SO_3^- group interference. The G-N1-Pt catalyst shown in Fig. 4(b) still effectively adsorbs hydrogen atoms, but at the same time, there are still two oxygen atoms in the SO_3^- group simultaneously adsorbed to the platinum atom at the active site, explaining the free energy rise of the reaction system. In the adsorption system under the catalytic action of G-N2-Pt catalyst, a hydrogen atom is adsorbed on one oxygen atom of the SO_3^- group, and the active site of Pt is occupied by another oxygen atom of the SO_3^- group (as shown in Fig. 4(c)). In the adsorption system under the catalytic action of G-N4-Pt catalyst, the hydrogen atom is also adsorbed on one oxygen atom of the SO_3^- group, and the SO_3^- group adsorbed with the hydrogen atom is desorbed on the catalyst surface as a whole (as shown in Fig. 4(d)). The above situation shows that these two catalysts are difficult to complete normal catalytic work under the interference of SO_3^- groups.

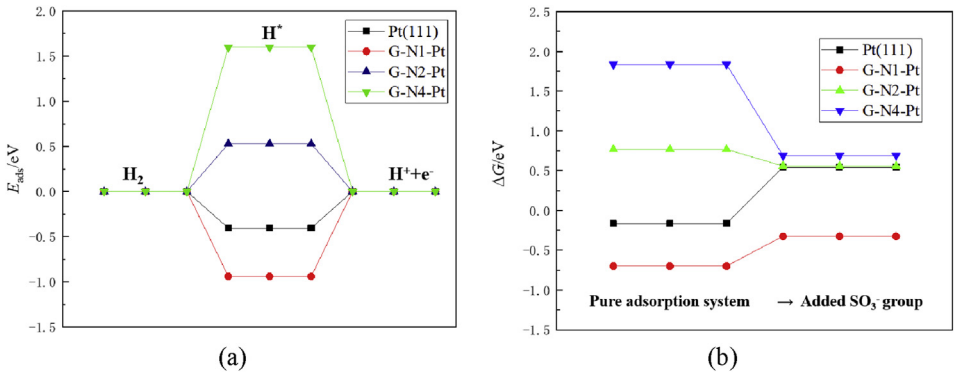

Fig. 3 – Comparison of HOR adsorption energy step diagrams of different catalysts (a) and activation free energy before and after interference with SO_3^- groups (b).

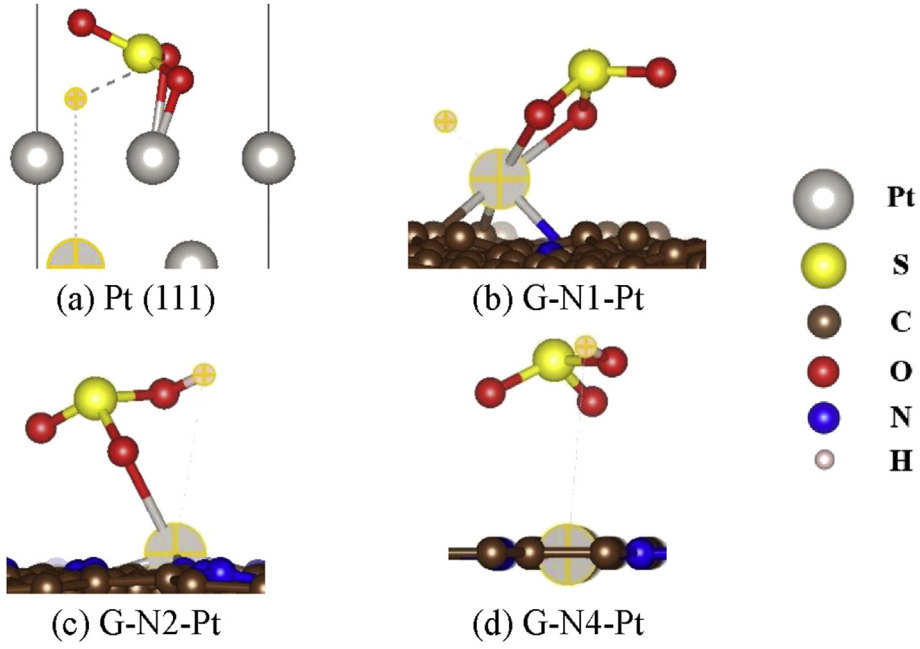

Fig. 4 – Adsorption of hydrogen atoms on G-N2-Pt (a) and G-N4-Pt (b) catalysts under SO_3^- interference.

Combining the electrocatalytic performance and anti-interference performance of the above four catalysts, it can be clearly seen that the G-N1-Pt catalyst has the best comprehensive performance. It has good catalytic performance itself, and at the same time, it can maintain acceptable electrochemical reaction ability under the interference of SO_3^- group.

ORR reaction analysis

After calculating the system energy according to the calculation parameter settings in Computation of electrochemical reactions, the initial energy of each system is obtained. Then the VASPKIT software package is used to correct the free energy of the system after adsorption, the atoms except the adsorption body should be fixed in the calculation. The correction principle is to ignore the contribution of translation and rotation to free energy, and only consider the contribution of vibration to free energy. The contribution of three-dimensional degrees of freedom vibration to free energy is calculated at room temperature (298.15 K). The free energy correction value is added to the initial energy of the system to obtain the corrected energy of the system. After the energy of each intermediate system in the reaction process is obtained, the energy of the non-adsorbed body in each intermediate process needs to be additionally added because they exist in the system during the reaction though they do not participate in the reaction. The non-adsorbed group contains water molecules (H_2O), oxygen molecules (O_2), hydrogen molecules (H_2) and hydrogen atoms (H). The specific energy values are provided in Table 3, where the hydrogen atom energy is calculated as 1/2 of the hydrogen molecule energy.

Table 3 – Non-adsorbed group energy.

System	H_2	O_2	H_2O
Optimized energy/eV	−6.8	−9.92	−14.22

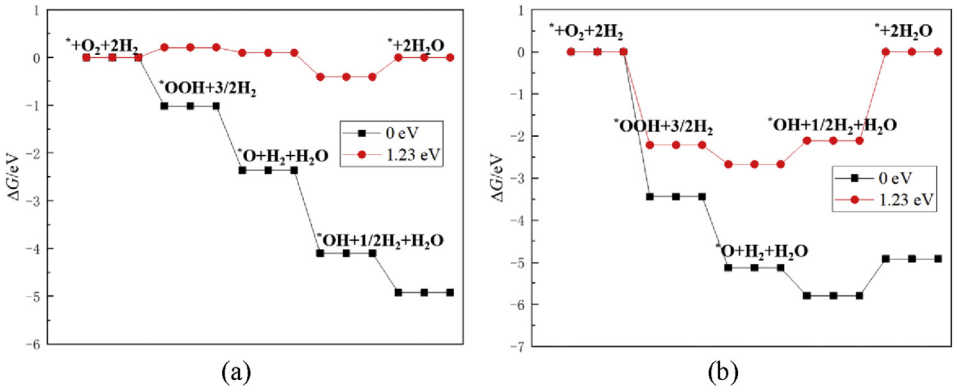

Fig. 5 – ORR reaction step diagram without (a) or with (b) SO_3^- groups on Pt (111) catalyst.

ORR reaction process under Pt (111) catalyst

The step diagram of the free energy of the reaction using Pt (111) catalyst is shown in Fig. 5(a) and the step diagram of the free energy of the reaction with the SO_3^- group is shown in Fig. 5(b). In Fig. 5(a), the black line is the system energy trend when the external additional voltage is 0 eV, and the red line indicates the system energy trend when the external additional voltage is 1.23 eV. The ORR reaction is an exothermic reaction. When the external voltage condition is 0 eV, the trend of the overall step diagram tends to be downward, and the system free energy range is 0 eV to −4.92 eV. Since there are 4 intermediate reaction steps in the ORR reaction, ideally the average free energy drop for each intermediate reaction step should be 1.23 eV. Therefore, in order to obtain the step diagram when the external additional voltage is 1.23 eV, it is necessary to add 1.23 eV to the energy of the intermediate reaction in each step.

But in fact, each step of the free energy in the ORR reaction will not be distributed so uniformly. During the standard ORR reaction of the conventional platinum particle catalyst/Pt (111) surface, the energy of the reaction step decreased steadily, and the energy of each reaction step decreases with 1.23 eV close to the ideal. The ORR reaction proceeded smoothly when catalyzed by the traditional platinum particle catalyst/Pt (111) surface, proving its good electrochemical performance. Under the condition of 1.23 eV of externally added voltage, the overall step diagram curve tends to be horizontal, indicating that the reaction proceeds more smoothly when there is externally applied voltage, and there is no obvious reaction barrier.

When SO_3^- group interference is introduced into the ORR reaction system on the Pt (111) surface, it can be seen that the overall step diagram has a significant sink (as shown in Fig. 5(b)), there is a clear difference from the situation where the energy decreases uniformly under standard reaction conditions. It can also be seen from Fig. 5(b) that when the external additional voltage is 0 eV, the energy of the reaction in the second step is already lower than −4.92 eV, and the energy of the system continues to decrease in the third step of the reaction. The energy rises instead when the reaction is completed. The free energy path of this reaction is also abnormal. At this time, the model diagram of the adsorption system introduced under the interference of the SO_3^- group (shown in Fig. 6) is further analyzed.

It can be seen in Fig. 6(a) that in the first step of the reaction, the hydroxide in the OOH^- group is adsorbed by the nearby SO_3^- group, while the two oxygen atoms of the SO_3^- group itself are adsorbed on two active sites on Pt (111) surface. In the second step reaction shown in Fig. 6(b), the SO_3^- group still has two oxygen atoms adsorbed on the active site, and the oxygen atoms participating in the reaction are simultaneously adsorbed by the catalyst and the SO_3^- group. In the third step reaction shown in Fig. 6(c), the hydroxides participating in the reaction are adsorbed by the SO_3^- group, which also cannot be normally adsorbed on the active site of the catalyst. It can be seen from the above analysis that the Pt (111) surface has lost the control of the intermediate adsorbent of the ORR reaction when it is disturbed by the SO_3^- group.

ORR reaction process under G-N1-Pt catalyst

The step diagram of the free energy of the reaction using G-N1-Pt catalyst is shown in Fig. 7(a) and the step diagram of the free energy of the reaction with the SO_3^- group is shown in Fig. 7(b).

It can be seen in Fig. 7(a), during the reaction on the surface of the G-N1-Pt catalyst, the distribution of the total free energy decrease is uniform, and the reaction can proceed smoothly. All these indicate that the G-N1-Pt catalyst has good ORR reaction catalytic performance. It is worth noting that the energy reduction in the first and second reaction steps of the G-N1-Pt catalyst reaction is significantly higher than that of the platinum particle catalyst/Pt (111) surface. This shows that in the overall reaction process, the first and second reactions are easier to carry out. Since the intermediate steps of the reaction are carried out in sequence, the higher energy reduction of the first and second steps has a positive effect on the progress of the overall ORR reaction.

However, under the interference of the SO_3^- group, the free energy drop in the first step of the reaction is greatly reduced, and the free energy drop in the second step is increased (as shown in Fig. 7(b)). At the same time, there is a high energy barrier of 1.993 eV in the third step of the reaction when the external additional voltage is 1.23 eV. These changes are due to the fact that the active site also absorbs interfering SO_3^-

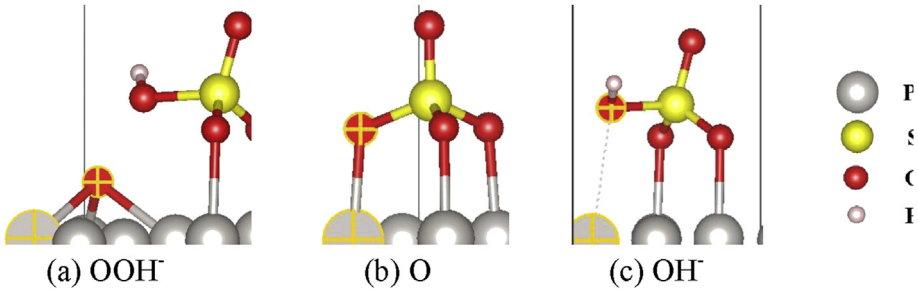

Fig. 6 – Adsorption of hydrogen peroxide (a), oxygen atom (b) and hydroxide (c) on Pt (111) surface under SO_3^- interference.

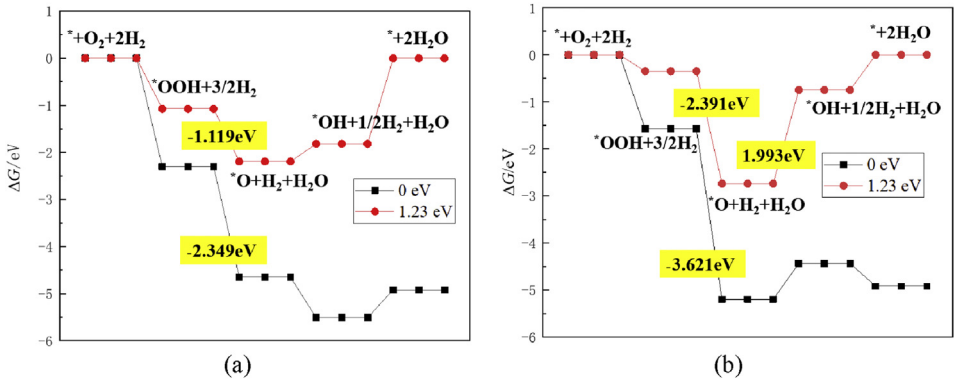

Fig. 7 – ORR reaction step diagram without (a) or with (b) SO_3^- groups on G-N1-Pt catalyst.

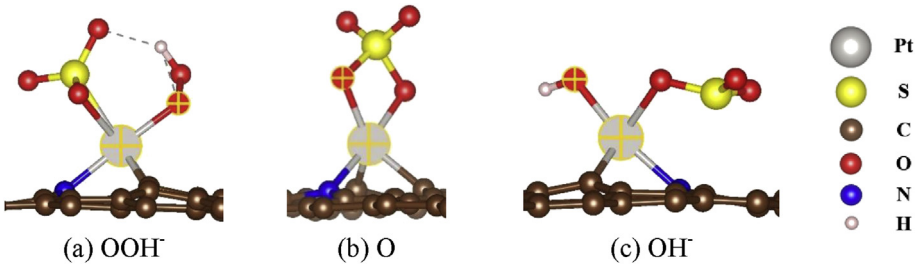

Fig. 8 – Adsorption of hydrogen peroxide (a), oxygen atom (b) and hydroxide (c) on G-N1-Pt active sites under SO_3^- interference.

groups in the intermediate electrochemical reaction (as shown in Fig. 8).

It can be seen that during the first reaction shown in Fig. 8(a), an oxygen atom and a sulfur atom in the SO_3^- group, and a hydrogen peroxide are simultaneously adsorbed on the Pt active site, which explains why the free energy drop in the first step of the reaction is reduced. However, when the hydroxide radical is desorbed from the hydrogen peroxide in the first step, the SO_3^- group and the Pt active site develop into a relatively balanced state, and two oxygen atoms are adsorbed at the same time (as shown in Fig. 8(b)). The stability of the system is greatly improved compared to the first step of the reaction, so the activity energy drop in the second step of the reaction is greatly increased. In the third step reaction shown in Fig. 8(c), although the SO_3^- group and the hydroxyl group are simultaneously adsorbed on the Pt active site, they repel each other. The hydroxide has only one oxygen atom adsorbed on Pt. At this time, the instability of the system increases significantly, so a high reaction energy barrier is generated.

In general, after SO_3^- group participates in the reaction, the SO_3^- group and the intermediate adsorbent are simultaneously adsorbed on the active site and have a repulsive relationship in space, which will have a great negative impact on the system stability of the intermediate process. The step diagram itself is based on the premise that the reaction can proceed smoothly, but judging from the actual intermediate step adsorption, the effect of SO_3^- on the reaction is likely to cause the reaction to fail.

ORR reaction process under G-N2-Pt catalyst

Fig. 9 shows the ORR reaction step diagram under the action of G-N2-Pt catalyst and the reaction step diagram under the interference of SO_3^- groups. It can be clearly seen in Fig. 9(a) that under the catalysis of G-N2-Pt, the free energy of the

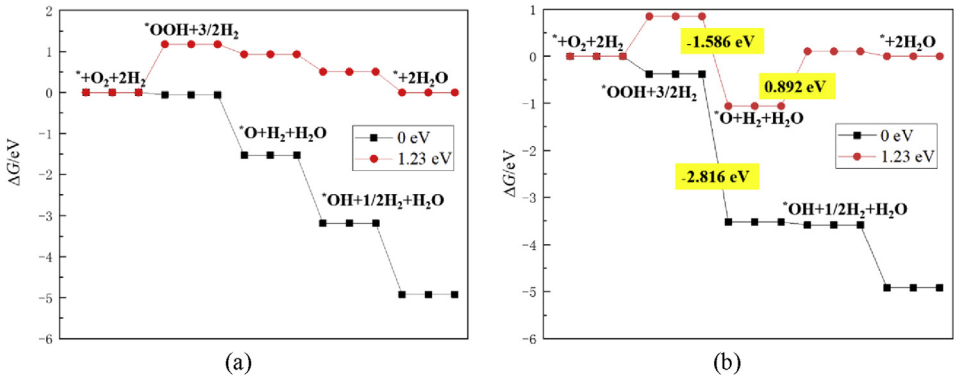

Fig. 9 – ORR reaction step diagram without (a) or with (b) SO_3^- groups on G-N2-Pt catalyst.

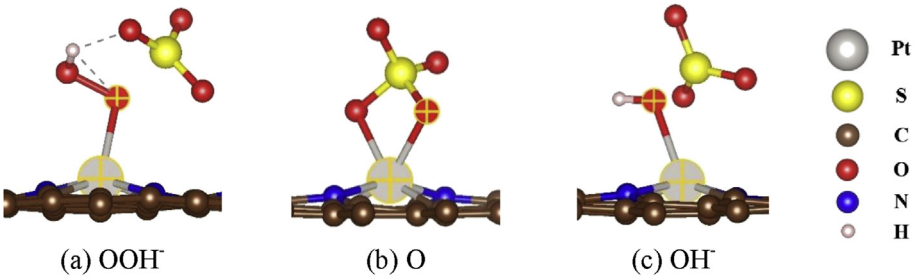

Fig. 10 – Adsorption of hydrogen peroxide (a), oxygen atom (b) and hydroxide (c) on G-N2-Pt active sites under SO_3^- interference.

entire ORR reaction system continues to decrease uniformly at external voltage 0 eV condition. At external voltage 1.23 eV condition shown in Fig. 9(b), the external potential can help the free energy to break through the reaction barrier in the first reaction step, and then the free energy continues to decrease so that the reaction can proceed smoothly.

After adding SO_3^- group to the system, the free energy of the reaction system at 0 eV still shows a continuous decline, which is better than other catalysts. However, the reaction needs to overcome the energy barrier two times in the first and third reaction steps at 1.23 eV, indicating that the reaction is still affected. Fig. 10 shows the adsorption of ORR intermediate reaction when a G-N2-Pt catalyst is used under the interference of SO_3^- groups. It can be seen that, compared with G-N1-Pt, the G-N2-Pt catalyst shows better anti-interference ability. In the first and third steps of the reaction (as shown in Fig. 10(a) and (b)), none of the SO_3^- groups adsorbed with the Pt active site, but the same situation as in the G-N1-Pt catalyst occurs in the second reaction step (shown in Fig. 10(b)). Two oxygen atoms simultaneously adsorb with the platinum and sulfur atoms.

ORR reaction process under G-N4-Pt catalyst

The ORR reaction step diagram using G-N4-Pt as the catalyst is shown in Fig. 11. It can be seen in Fig. 11(a) that under the condition of 0 eV, the free energy of the first reaction step is a rising state, which means that the first step of the reaction requires external energy to help it complete. This means that

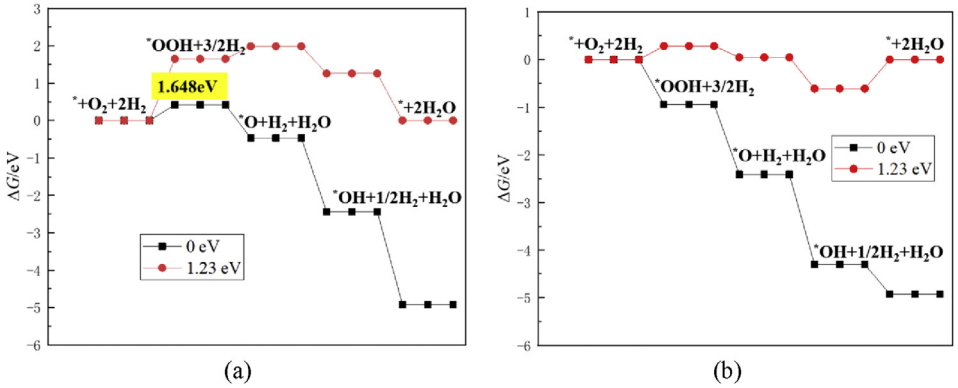

Fig. 11 – ORR reaction step diagram without (a) or with (b) SO_3^- groups on G-N4-Pt catalyst.

certain conditions are required to start the ORR reaction, and the reaction itself is relatively difficult to achieve. Under the condition of 1.23 eV, the free energy growth in the first step of the reaction is also raised to 1.648 eV, which also requires additional energy to proceed.

When SO_3^- group interference is introduced into the system, Fig. 11(b) reflects that the free energy of ORR reaction under the action of G-N4-Pt catalyst decreases evenly at 0 eV condition, while at an externally applied voltage of 1.23 eV, the highest reaction energy barrier in the intermediate step of the reaction is 0.61 eV which can be easily solved by external voltage. The result of the energy change in the step diagram shows that the SO_3^- group not only does not interfere with the reaction process, but promotes the reaction process positively. This rule does not meet the expected judgment, and further judgments need to be made in conjunction with the intermediate reaction system diagram.

It can be seen in Fig. 12(a) that in the first step of the reaction, the hydrogen peroxide is adsorbed by the SO_3^- group and detached from the catalyst surface. This means that under the interference of the SO_3^- group, the first step of the reaction is greatly disturbed and difficult to proceed. When the first step of the reaction is difficult to proceed, the progress of the overall ORR reaction is bound to be greatly hindered. Not only that, in the second step of the reaction shown in Fig. 12(b), the oxygen atom at the activation site is also adsorbed by the SO_3^- group. In the third step of the reaction shown in Fig. 12(c), the hydroxide ions are adsorbed by the SO_3^- group and desorbed to the active site of the catalyst as in the first step. The above adsorption conditions show that the interference of SO_3^- groups has a great impact on the actual performance of G-N4-Pt catalyst.

Analysis and summary

The electrochemical performance and anti-interference ability of the four catalysts are shown and compared in HOR reaction analysis and ORR reaction analysis. The calculation results are further combed and analyzed in this section.

For HOR reaction, both the Pt (111) surface and G-N1-Pt have good catalytic performance under standard reaction conditions. The surface of Pt (111) itself has a large number of active sites, and it is amiable to adsorb hydrogen atoms during the reaction. The adsorption sites are also diverse on Pt (111) surface, and each adsorption site has a strong adsorption energy. The G-N1-Pt catalyst has a prominent platinum atom position in its configuration, so it is also amiable to adsorb hydrogen atoms in the reaction, making it have good electrocatalytic performance. When the interference of SO_3^- group is introduced into the HOR reaction system, the catalytic performance of Pt (111) surface decreases significantly. This is because its abundant active sites not only provide favorable conditions for the adsorption of hydrogen atoms, but also adsorb SO_3^- groups. The G-N2-Pt and G-N4-Pt catalysts perform poorly when the HOR reaction is interfered by SO_3^- groups. This is because more nitrogen atoms in the substrate provide better structural stability (which can be seen from their planar structures), but also weaken its adsorption and catalytic ability. In comparison, G-N1-Pt catalyst has a balance between activation performance and stability, so it has excellent catalytic performance in both standard reaction conditions and reactions with SO_3^- interference.

For the ORR reaction, the performance difference of each catalyst under standard reaction conditions is reduced. This is because in the ORR reaction, both the adsorbate and the catalyst are connected by a platinum-oxygen (Pt–O) bond with higher bond energy than platinum-hydrogen (Pt–H) bond.

The Pt (111) surface exhibits excellent ORR catalytic performance under standard operating conditions. When the external additional voltage is 0 eV, the energy of each step of the reaction decreases evenly. When the external additional voltage is 1.23 eV, the reaction step diagram is approaching the horizontal, indicating that there is no need for excessive external voltage to assist in the reaction. However, when SO_3^- group is added to interfere, the large number of active sites on the surface of Pt (111) also provides good adsorption conditions for SO_3^- group. After stably adsorbed on the surface of Pt (111), SO_3^- group directly adsorbs the reaction adsorbate, especially has a strong adsorption capacity for OH^- group. At this time, the surface of Pt (111) becomes the standpoint of SO_3^- group, which makes the SO_3^- group more stable in the system, but has a more serious negative effect on the normal ORR reaction process.

Since the platinum-oxygen bond strength is higher in the ORR reaction compared with the platinum-hydrogen bond in the HOR reaction, the weakening effect of the nitrogen atom in the catalyst substrate on the activation performance of the platinum atom is reduced, and G-N2-Pt has a better effect in the ORR reactionperformance. However, among the three single-atom catalysts, the G-N4-Pt catalyst is still the worst

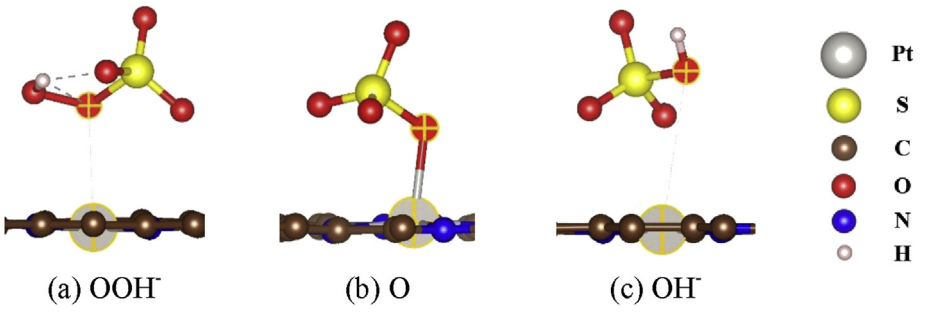

Fig. 12 – Adsorption of hydrogen peroxide (a), oxygen atom (b) and hydroxide (c) on G-N4-Pt active sites under SO_3^- interference.

performing catalyst, requiring a higher initial voltage when performing the reaction, which means the required reaction conditions are more stringent than those of G-N1-Pt and G-N2-Pt catalysts. This indicates that the nitrogen atoms in the substrate still affect the activation performance of platinum atoms to some extent. At the same time, the SO_3^- group also easily replaces the reactant to form a platinum-oxygen bond with the platinum atom at the active site, thereby affecting the performance of the G-N1-Pt catalyst with prominent platinum atom sites. In the reaction, the SO_3^- group is more easily adsorbed on the protruding platinum atoms, which results in the G-N1-Pt catalyst having insufficient anti-interference ability in the ORR reaction. The G-N2-Pt catalyst substrate has a moderate amount of doped nitrogen atoms which ensures its sufficient catalytic activity. At the same time, its planar configuration makes it difficult to adsorb SO_3^- groups and the intermediate adsorbent simultaneously from the spatial position. By achieving the optimal balance between structure and activation performance, G-N2-Pt catalyst exhibits the best comprehensive catalytic ability and anti-interference ability in the ORR reaction.

To sum up, for HOR reaction, the catalyst with the best combination of catalytic ability and anti-interference ability is G-N1-Pt catalyst, and for ORR reaction, the best performance is G-N2-Pt catalyst. It can be found from the analysis that the strength and process of the HOR and ORR reactions are different, so the emphasis is different when selecting a catalyst. It can be found in the calculation results and the literature [23,24,29] that single-atom catalysts have many advantages over traditional platinum particle catalysts, such as low platinum loading and strong functionality. When constructing a single-atom catalyst, if only from the perspective of catalytic performance, it is desirable that the active sites in the catalyst be as prominent as possible, and it is liable to react with the reactants. For the HOR and ORR reaction in a fuel cell, it is also necessary to consider the electrochemical damage and interference that may occur during the work process. The position structure of the active site needs to be balanced so that it has both catalytic performance and anti-interference ability.

Conclusions

In this paper, common-used Pt (111) catalyst and three single-atom catalysts: G-N1-Pt, G-N2-Pt, and G-N4-Pt are studied based on first principle method. Based on the electrochemical damage of fuel cells, the effects of different catalysts on HOR and ORR reactions under standard operating conditions and interference with SO_3^- groups are discussed. Here are the conclusions:

(1) It is proposed that the SO_3^- group in the proton exchange membrane will directly affect the electrochemical reaction inside the catalyst layer when the interface between the proton exchange membrane and the catalyst is blended. The SO_3^- group is weakly bonded to the main bond in the molecular chain, and is located on the periphery of the molecular chain as a branch, easily contacting the internal structure of the catalytic layer. Moreover, the oxygen atoms at the top of the SO_3^- group easily reacts and adsorbs with the platinum atom at the active site in the catalyst. Based on this viewpoint, the electrochemical reaction under the interference of SO_3^- group is modeled and compared with the reaction under standard condition.

(2) In the standard HOR reaction, the platinum-hydrogen bond energy in the HOR reaction is weak, so the catalyst activity is required to be high. Pt (111) surface and G-N1-Pt catalyst perform best among the four catalysts. This is due to the abundant activation sites in Pt (111) and the prominent activation sites in the G-N1-Pt catalyst. When SO_3^- group interference is introduced, Pt (111) surface's abundant activation sites make it easy to adsorb with SO_3^- group, which becomes a disadvantage and reduces its performance. In comparison, the G-N1-Pt catalyst is less affected and the reaction free energy rise is smaller, indicating that it has the best comprehensive ability in HOR reaction.

(3) In the ORR reaction, the platinum-oxygen bond formed between the catalyst surface and the adsorbent is stronger than the platinum-hydrogen bond, so the catalyst activity requirement is reduced compared to the HOR reaction. The three catalysts Pt (111), G-N1-Pt and G-N2-Pt all have good performance. The reaction step diagram shows a steady downward trend, indicating that the reaction is going smoothly. The interference effect of the introduced SO_3^- group is still obvious. The SO_3^- group on the surface of the Pt (111) catalyst is prone to stable adsorption, and then captures the OH^- group and oxygen atom in the reaction process, causing serious damage to the reaction. In the intermediate reaction step of the G-N1-Pt catalyst, the SO_3^- group and the intermediate adsorbent are simultaneously adsorbed on the protruding platinum atom sites, which has a certain negative effect on the reaction. The G-N2-Pt catalyst exhibits good anti-interference performance and shows repulsion to SO_3^- group.

(4) Combining the above results to analyze the anti-interference performance of the catalyst, when considering external interference, it is necessary to balance the relationship between the arrangement of active site and the stable structure. The arrangement of protruding or exposed active sites is easy for intermediate adsorption, and it is also more susceptible to interference. The most prominent advantage of platinum particle catalysts is their abundant active sites, but this becomes a disadvantage when faced with interference. In this respect, the single-atom catalyst itself has certain advantages over traditional platinum particle catalysts. According to different requirements of different reactions, different treatments are also needed in the structural design of catalysts. In the HOR reaction, due to the weak hydrogen bond strength of platinum, the position of the platinum atom needs to be placed in a more prominent position of single-atom catalysts. In the ORR reaction, the strength of the platinum-oxygen bond is high, so there is no need to perform structural protruding treatment on the single-

atom catalyst, and it also needs to ensure a certain activity strength and reaction stability.

Data availability statements

The data that supports the findings of this study are available in the paper.

Acknowledgements

This study is funded by the National Natural Science Foundation of China 51876161.

REFERENCES

[1] Mohsin M, Raza R, Mohsin-ul-Mulk M, et al. Electrochemical characterization of polymer electrolyte membrane fuel cells and polarization curve analysis. Int J Hydrogen Energy 2020;45(29):14953–63.
[2] Lü X, Qu Y, Wang Y, Qin C, et al. A comprehensive review on hybrid power system for PEMFC-HEV: issues and strategies. Energy Convers Manag 2018;171:1273–91.
[3] Zhang SS, Yuan XZ, Wang HJ, et al. A review of accelerated stress tests of MEA durability in PEM fuel cells. Int J Hydrogen Energy 2009;34(1):388–404.
[4] Borup R, Meyers J, Pivovar B, et al. Scientific aspects of polymer electrolyte fuel cell durability and degradation. Chem Rev 2007;107:3904–51.
[5] Wang C, Wang SB, Zhang JB, et al. The durability research on the proton exchange membrane fuel cell for automobile application. Prog Chem 2015;27:424–35.
[6] Li Y, Moriyama K, Gu W, Arisetty S, Wang CY. A one-dimensional Pt degradation model for polymer electrolyte fuel cells. J Electrochem Soc 2015;162:F834–42.
[7] Urchaga P, Kadyk T, Rinaldo SG, et al. Catalyst degradation in fuel cell electrodes: accelerated stress tests and model-based analysis. Electrochim Acta 2015;176:1500–10.
[8] Zhao M, Shi WY, Wu BB, et al. Influence of membrane thickness on membrane degradation and platinum agglomeration under long-term open circuit voltage conditions. Electrochim Acta 2015;153:254–62.
[9] Shibaguchi T, Sugiura T, Fujitsu T, Nomura T, Ohira Y. Effects of icing or heat stress on the induction of fibrosis and/or regeneration of injured rat soleus muscle. J Physiol Sci 2016;66:345–57.
[10] Vasić DD, Pašti IA, Mentus SV. DFT study of platinum and palladium overlayers on tungsten carbide: structure and electrocatalytic activity toward hydrogen oxidation/evolution reaction. Int J Hydrogen Energy 2013;38(12):5009–18.
[11] Haddad AZ, Garabato BD, et al. Beyond metal-hydrides: non-transition-metal and metal-free ligand-centered electrocatalytic hydrogen evolution and hydrogen oxidation. J Am Chem Soci 2016:6b04441.
[12] Lozano T, Rankin RB. Computational predictive design for metal-decorated-graphene size-specific SubNanometer to nanometer ORR catalysts. Catal Today 2018;312.
[13] Nigam Sandeep, Majumder Chiranjib. ORR viability of alumina supported platinum nanocluster: exploring the oxidation behaviour by DFT methods. Phys Chem Chem Phys 2017;19(29):19308.
[14] Yin Y, Wang J, Yang X, et al. Modeling of high temperature proton exchange membrane fuel cells with novel sulfonated polybenzimidazole membranes. Int J Hydrogen Energy 2014;39(25):13671–80.
[15] Akita T, Taniguchi A, Maekawa J. Analytical TEM study of Pt particle deposition in the proton-exchange membrane of a membrane-electrode-assembly. J Power Sources 2006;159(1):461–7.
[16] Mauritz KA, Moore RB. State of understanding of nafion. Chem Rev 2004;104(10):4535–85.
[17] Lee HJ, Cho MK, Jo YY, et al. Application of TGA techniques to analyze the compositional and structural degradation of PEMFC MEAs. Polym Degrad Stabil 2012;97(6):1010–6.
[18] Material Studio software, 2019. https://www.3dsbiovia.com/products/collaborative-science/biovia-materials-studio/.
[19] Kresse G, Furthmüller J. Efficiency of ab-initio total energy calculations for metals and semiconductors using a plane-wave basis set. Comput Mater Sci 1996;6(1):15–50.
[20] Wang V, Xu N, Liu JC, et al. VASPKIT: a pre- and post-processing program for VASP code. Condensed Matter arXiv:1908 2019. 08269.
[21] Momma K, Izumi F. VESTA: a three-dimensional visualization system for electronic and structural analysis. J Appl Crystallogr 2008;41(3):653–8.
[22] Duan S, Wang R, Liu J. Stability investigation of a high number density Pt1/Fe2O3 single-atom catalyst under different gas environments by HAADF-STEM. Nanotechnology 2018;29.
[23] Cao XR, Ji YF, Luo Y. Dehydrogenation of propane to propylene by a Pd/Cu single-atom catalyst: insight from first-principles calculations. J Phys Chem C 2015;119(2):1016–23.
[24] He BL, Shen JS, Tian ZX. Iron-embedded C2N monolayer: a promising low-cost and high-activity single-atom catalyst for CO oxidation. Phys Chem Chem Phys 2016;18(35):24261.
[25] Norskov JK, Abild-Pedersen F, Studt F, et al. Surface Chemistry Special Feature: density functional theory in surface chemistry and catalysis. Proc Natl Acad Sci USA 2011;108(3):937–43.
[26] Norskov JK, Bligaard T, Logadottir A, et al. Trends in the exchange current for hydrogen evolution. ChemInform 2005;36(24). e12154-e12154.
[27] Norskov JK, Rossmeisl J, Logadottir A, et al. Origin of the overpotential for oxygen reduction at a fuel-cell cathode. J Phys Chem B 2004;108(46):17886–92.
[28] Liu J, Jiao M, Lu L, et al. High performance platinum single atom electrocatalyst for oxygen reduction reaction. Nat Commun 2017;8:15938.
[29] Fei H, Dong J, Feng Y, et al. General synthesis and definitive structural identification of MN4C4 single-atom catalysts with tunable electrocatalytic activities. Nature Catalysis 2018;1(1):63–72.